ChemPubSoc Europe

DOI: 10.1002/chem.201304393

CHEMISTRY A European Journal Full Paper

Stereochemistry

Absolute Stereochemistry of a 4a-Hydroxyriboflavin Analogue of the Key Intermediate of the FAD-Monooxygenase Cycle**

Soichiro Iwahana,[a] Hiroki Iida,[a] Eiji Yashima,*[a] Gennaro Pescitelli,[b] Lorenzo Di Bari,*[b] Ana G. Petrovic,[c, d] and Nina Berova*[c]

Dedicated to Professor Koji Nakanishi on the occasion of his 88th birthday

Abstract: The biological action of flavoenzymes, such as flavin adenine dinucleotide (FAD)-containing monooxygenase, involves the formation of oxygenated flavin derivatives, such as 4a-hydroperoxyflavin and 4a-hydroxyflavin, in which a new center of chirality is created at the 4a position during the enzymatic reactions. So far, the absolute configuration of this center of chirality in natural 4a-oxygenated flavins has remained unknown in spite of its key importance for the diverse functions of flavoenzymes. Herein, we report the 4a-hydroxy adduct **3** of 3-benzyl-5-ethyl-10-(tetraacetyl-D-ribityl)flavinium (**1**), one of the key intermediates involved in the enantioselective organocatalytic oxidation of sulfides to sulfoxides. The 4a-hydroxyflavin diastereomers (+)-**3** and (−)-**3**, separated by HPLC, were characterized by electronic circular dichroism (CD) spectroscopy. Their absolute configurations at the 4a position were, for the first time, determined by comparing experimental CD spectra with those calculated by means of time-dependent density functional theory (TDDFT) on DFT-optimized structures obtained after an extensive conformation analysis.

Introduction

Riboflavin (vitamin B_2) and its biologically active forms, flavin mononucleotide (FMN) and flavin adenine dinucleotide (FAD), play a central role in the oxidative degradation of xenobiotic substances as cofactors of flavoenzymes, such as the hepatic microsomal FAD-containing monooxygenase (FADMO), a class of ubiquitous redox-active enzyme.[1] The catalytic activity of FADMO relies on the formation of the key intermediate 4a-hydroperoxyflavin (FlOOH), generated from the oxidized flavin (Fl_{ox}) through conversion into the reduced flavin and the subsequent reaction with molecular oxygen, which promotes the monooxygenation of substrates, such as sulfides to sulfoxides. This process is accompanied by the formation of 4a-hydroxyflavin (FlOH), which simultaneously undergoes dehydration to regenerate Fl_{ox} (Scheme 1a).[2] This flavin-catalyzed oxidation mechanism has been widely accepted based on kinetic and spectroscopic studies on flavoenzymes,[2] but the key intermediate FlOOH has not yet been isolated as a structurally defined active species despite a number of flavoenzyme structures determined by X-ray analyses because it is extremely unstable outside of enzymes.[3]

Inspired by such intriguing and diverse functions of flavoenzymes, in particular FADMO, the design and synthesis of artificial flavin-based organocatalysts has become an attractive challenge not only to mimic and elucidate the flavin-mediated monooxygenation processes, but also to develop environment-friendly organocatalysts.[4] Since the pioneering work by Kemal and Bruice[1a,5] and Murahashi et al.,[6] who developed a versatile method to generate the oxidatively active 5-ethyl-4a-hydroperoxyflavin in situ from the corresponding flavinium cation in the presence of hydrogen peroxide (H_2O_2), which promotes the catalytic oxidation of sulfides and amines in a way similar to FADMO, a variety of chiral and achiral flavin-based organocatalysts have been synthesized for diverse transformation reactions, including the catalytic asymmetric oxidation of sulfides and the Baeyer–Villiger oxidation of ketones.[7] However, the key intermediates of the FlOOH type were not isolated and merely characterized by spectroscopic techniques,[5,6] and their molecular structures, including the stereochemistry at the 4a position, have never been determined.

We have recently reported an optically active riboflavin-based organocatalyst **1** readily derived from commercially

[a] S. Iwahana, Dr. H. Iida, Prof. E. Yashima
Department of Molecular Design and Engineering
Graduate School of Engineering
Nagoya University, Nagoya 464-8603 (Japan)
E-mail: yashima@apchem.nagoya-u.ac.jp

[b] Dr. G. Pescitelli, Prof. L. Di Bari
Department of Chemistry
University of Pisa, Via Risorgimento 35, 56126 Pisa (Italy)
E-mail: lorenzo.dibari@unipi.it

[c] Dr. A. G. Petrovic, Prof. N. Berova
Department of Chemistry, Columbia University
3000 Broadway 3114, New York, NY 10027 (USA)
E-mail: ndb1@columbia.edu

[d] Dr. A. G. Petrovic
Department of Life Sciences, New York Institute of Technology
1855 Broadway, New York, NY 10023 (USA)

[**] FAD = flavin adenine dinucleotide.

Supporting information for this article is available on the WWW under http://dx.doi.org/10.1002/chem.201304393.

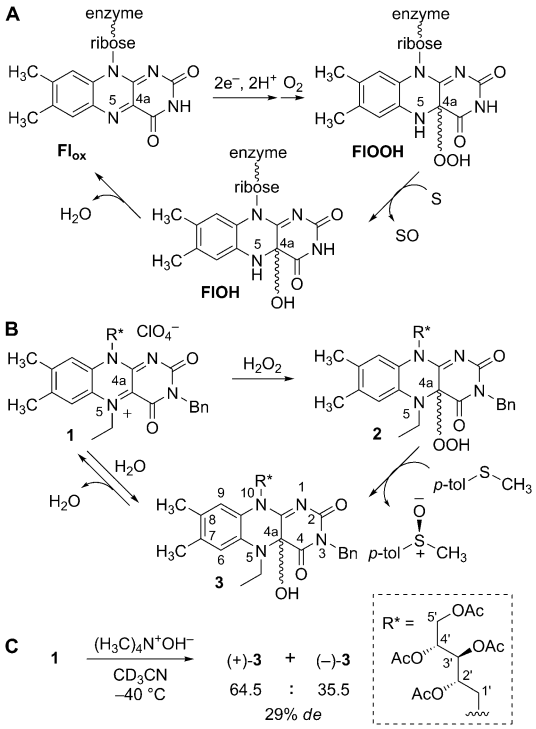

Scheme 1. a) Biological catalytic cycle for the FADMO-mediated oxidation of sulfides with molecular oxygen through the formation of FlOOH and FlOH. b) Biomimetic catalytic cycle for the 5-alkylated flavinium perchlorate **1**-mediated oxidation of sulfides with H_2O_2 through the formation of 4a-hydroperoxy **2** and 4a-hydroxy **3** adducts. The nucleophilic addition of H_2O to **1** also produces 4a-hydroxy **3**. c) Diastereoselective hydration of **1** with $Me_4N^+OH^-$ in CD_3CN at $-40\,^\circ C$. The prefixes + and − of **3** denote the signs of the optical rotation at the sodium D-line.

available riboflavin, which also promotes the asymmetric oxidation of methyl *para*-tolyl sulfide catalyzed by 4a-hydroperoxyflavin **2** generated in situ from the 5-ethylflavinium cation **1** by the nucleophilic addition of H_2O_2, thus giving the corresponding optically active (*S*)-methyl *para*-tolyl sulfoxide with up to 30% enantiomeric excess (*ee*) along with 4a-hydroxyflavin **3**, which further undergoes dehydration to regenerate cation **1** in the presence of $HClO_4$ to complete the biomimetic catalytic oxidation cycle (Scheme 1b).[8]

The enantioselectivity observed in the asymmetric oxidation was anticipated to closely link to the stereochemistry (diastereoselectivity) of 4a-hydroperoxyflavin **2** generated in situ. Various attempts to isolate **2** to determine the structure and estimate its diastereomeric excess (*de*) were unsuccessful because of its labile characteristics in solution. The 4a-hydroxyflavin compound **3** was also produced from **1** through a similar nucleophilic addition of H_2O (Scheme 1B) and was quite stable while maintaining its absolute configuration at the 4a position, which was identical to that of **2**. On the basis of this assumption, we performed the hydroxylation of **1** at the 4a position in the presence of $Me_4N^+OH^-$ in CD_3CN at $-40\,^\circ C$ and found that this reaction proceeded in a diastereoselective fashion, thus yielding a diastereomeric mixture of **3** (64.5:35.5; 29% *de*) as estimated from its ^1H NMR spectrum (Scheme 1c).[8]

In the present study, we synthesized and isolated the optically active 4a-hydroxyflavin diastereomers (+)- and (−)-**3** according to the previously reported method,[8] and investigated the effects of the stereogenic center at the 4a position (OH group) and the tetraacetyl-D-ribityl residue on the chiroptical properties of (+)- and (−)-**3**. Electronic circular dichroism (CD) spectra were measured and compared with CD calculations based on the time-dependent density functional theory (TDDFT) to determine the absolute configurations at the 4a positions of the (+)-**3** and (−)-**3** diastereomers.

Despite the key importance of 4a-oxygen adducts as active intermediates in a large family of ubiquitous flavoenzymes for diverse functions, the stereostructures of the 4a-oxygen adducts, in particular, the absolute configurations at the 4a position of flavoenzymes and those of the synthetic analogues, have never been unambiguously determined.[9] The present molecular-level stereochemical information will allow us to rationalize the previously reported enantioselectivity in the asymmetric oxidation of sulfides catalyzed by **1**,[8] to provide an important clue toward the elucidation of the mechanisms of flavin-catalyzed reactions, and to design novel chiral flavin-based organocatalysts with higher enantioselectivity.

Results

Chromatographic separation and characterization of (+)-3 and (−)-3

The 4a-hydroxy adduct **3** was successfully separated into diastereomers (+)-**3** and (−)-**3** by means of a chiral HPLC column (Chiralpak IB, Daicel Co., Ltd.) with *n*-hexane/$CHCl_3$ (1:1, v/v) as the eluent or an HPLC column (Cosmosil $5C_{18}$-MS-II, Nacalai Tesque) with acetonitrile (ACN)/H_2O (11:9, v/v) as the eluent (see Figure S1 A in the Supporting Information).

In the ^1H NMR spectra, diastereomers (+)-**3** and (−)-**3** may be easily identified in their mixtures by means of the aromatic protons H6 and H9, which appear as singlets at $\delta = 7.03$ and 7.23 ppm for (+)-**3** and $\delta = 7.05$ and 7.18 ppm for (−)-**3**, respectively (see Figure S1 B in the Supporting Information). In this way, the *de* values of (+)-**3** and (−)-**3** separated as described above were estimated to be 94% (see Figure S1 C and S1 D in the Supporting Information). In view of the subsequent theoretical conformation analysis, variable-temperature (VT) ^1H NMR spectra and nuclear Overhauser effect spectroscopy (NOESY) spectra were recorded in CD_3CN to obtain information about the preferential conformations assumed by (+)-**3** and (−)-**3** in solution. In particular, we were interested in any clue about the possible formation of intramolecular hydrogen bonds between the 4a-OH group and one or more acetyl groups on the tetraacetyl-D-ribityl moiety, as evidenced by preliminary modeling results (see below). As expected, the 4a-OH protons of (+)-**3** and (−)-**3** in CD_3CN (2 mM) were monotonically shifted downfield upon heating; the chemical shifts changed from $\delta = 4.58$ ppm at 303 K to $\delta = 4.41$ ppm at 343 K for both (+)-**3** and (−)-**3**. A linear δ (in ppm) versus T (in K) relationship was observed in both cases with a temperature coefficient $\Delta\delta/\Delta T$ (linear-fit slope) of −4.3 and −4.4 ppb K^{-1} for (+)-**3** and

(−)-**3**, respectively (see Figure S2A and S2B in the Supporting Information). These data exclude the possibility that the 4a -OH protons of (+)-**3** and (−)-**3** are involved in any intramolecular hydrogen bonds.[10] This assumption was supported by the facts that *tert*-butanol (40 mM in CD_3CN) gave a similar coefficient of -4.8 ppb K^{-1} (see Figure S2C in the Supporting Information) and no NOE correlations could be detected between the protons that lie on the 4a-hydroxyflavin moiety and any of the acetyl protons of **3**.[8] As we shall discuss more in detail below, such intramolecular hydrogen bonds would involve the formation of a medium-size ring, which is disfavored in itself and becomes even less likely on account of the polarity and the fairly good hydrogen-bond-acceptor character of the solvent ACN ($\beta = 0.40$).[11]

The absorption and electronic CD spectra of (+)-**3** and (−)-**3** were measured in ACN to investigate the effects of the chirality at the 4a position on their chiroptical properties (Figure 1).

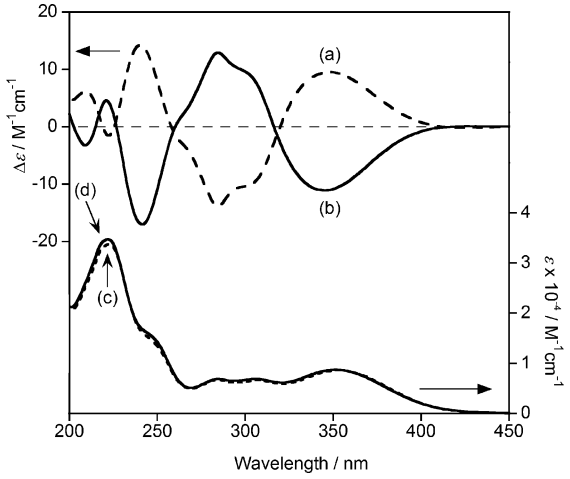

Figure 1. a,b) CD and c,d) absorption spectra of (+)-**3** (a,c) and (−)-**3** (b,d) in ACN at approximately 25 °C. The concentrations of (+)- and (−)-**3** were 0.5 mM and their *de* values were 94%.

The absorption spectra of the two diastereomers were almost identical and showed a manifold of bands in the region of $\lambda =$ 200–450 nm allied with the 4a-hydroxyflavin and benzene chromophores. In the CD spectra, (+)-**3** and (−)-**3** (both with 94% *de*) showed intense bands of alternating sign centered at around $\lambda = 348$, 285, and 240 nm and weaker bands at shorter wavelengths. Very interestingly, the two diastereomers were associated with almost mirror-image CD patterns. The mirror-image relationship was not perfect, as evidenced by slightly different absolute values of the CD intensities and by the observation that the two spectra do not cross exactly at zero values. Still, the spectra clearly suggested that the chiroptical properties of the diastereomers are significantly governed by the chirality at the 4a position and that the contribution from the tetraacetyl-D-ribityl group is negligibly small. In other words, the two diastereomers behave almost as pseudoenantiomers from the viewpoint of their electronic CD spectra. We measured concentration-dependent absorption and CD spectra of (−)-**3** to highlight possible aggregation phenomena. However, the magnitudes of the CD and absorption signals of (−)-**3** (in $M^{-1}cm^{-1}$) were hardly changed over the concentration range from 0.0125 to 0.5 mM in ACN, thus indicating that the formation of aggregates could be excluded (see Figure S3 in the Supporting Information). With hope of detecting a chiroptical property more sensitive to the diasteromeric nature of the compounds, we attempted to measure vibrational circular dichroism (VCD) spectra of (+)-**3** and (−)-**3** in ACN. However, no diagnostic signals could be detected in the IR regions of the 4a-hydroxyflavin residue.

Molecular modeling study of (*S*)-3

Following a common protocol for the simulation of CD spectra of flexible organic molecules,[12] we first carried out an exhaustive molecular-modeling investigation to establish the most probable solution conformations of **3**, which were to be used as input structures in the CD calculations. This protocol first encompasses a comprehensive conformational search run with molecular-mechanics calculations, followed by DFT geometry optimizations of the various identified conformers.

Structures with an arbitrarily chosen configuration (4a*S*) were considered in the modeling. The starting structure of (*S*)-**3** was built based on the combination of two reported X-ray crystallographic structures, one with coordinates provided for the 5-ethyl-4a-hydroxyflavin segment of 5-ethyl-4a-hydroxy-3-methyl-lumiflavin and the second with coordinates taken from the tetraacetyl-D-ribityl segment of riboflavin tetraacetate[13] by addition of a benzyl moiety at N3. This starting geometry of (*S*)-**3** was subjected to a series of Monte Carlo (MC) conformational search algorithms in vacuo (see the Computational Section). The MC search provided a pool of approximately 3000 conformers, which was narrowed down to 25 distinct representative structures based on the redundant-conformer elimination method (see the Computational Section for details). Among the representative 25 structures, 12 conformers (henceforth indicated as "closed" structures, (*S*)-$\mathbf{3_C}$) showed intramolecular hydrogen bonding between the 4a-OH moiety and one of the C=O groups attached to the D-ribityl unit at positions 2′, 4′, or 5′. The remaining 13 conformers showed no intramolecular hydrogen bonding (indicated as "open" structures; i.e.,
(*S*)-$\mathbf{3_O}$), and the majority of these conformers had the 4a-OH group and the tetraacetyl-D-ribityl side chain on opposite sides of the flavin ring. The 25 unique conformations identified by the MC search were submitted to geometry optimization and frequency calculation by using DFT methods at the B3LYP/6-31G(d) level of theory in the gas phase. Surprisingly, DFT-optimized hydrogen-bonded (*S*)-$\mathbf{3_C}$ conformers were much more stable than the (*S*)-$\mathbf{3_O}$ conformers. Based on the relative free energies, the overall Boltzmann population at 300 K for the hydrogen-bonded (*S*)-$\mathbf{3_C}$ conformers was as high as 94.4% (see Table S1 in the Supporting Information for a list of the calculated free energies and populations). To ascertain possible errors related to the employed functional and basis set, the two most stable structures belonging to the "open" and "closed" families

(indicated as **C12$_o$** and **C2$_c$** in Table S1, respectively) were reoptimized at the M06-2X/6-311+G(d,p) level. The reoptimization did not substantially change the free-energy difference between the two structures (see Table S2 in the Supporting Information). This finding that the most stable conformations calculated for (*S*)-**3** possessed an intramolecular hydrogen bond not only contradicted the NMR spectroscopic data discussed above, but was also hard to reconcile with the experimental CD data. In fact, any strong interaction between the tetraacetyl-D-ribityl and 4a-hydroxyflavin moieties would be expected to produce sizable differences in the CD profiles for the two diastereomers, which was not the case.

Next, we explored the possibility that the theoretically overpredicted stability of the hydrogen-bonded (*S*)-**3$_c$** conformers could be a computational artifact due to the absence of a solvent environment. Therefore, we first attempted to use an implicit solvent model by running a single-point-energy calculation on the pool of 25 conformers at the M06-2X/6-311+G(d,p) level of theory by employing the integral equation formalism polarizable continuum model (IEF-PCM) for ACN.[14] Once again, however, the overall population calculated with M06-2X/6-311+G(d,p)[IEF-PCM]//B3LYP/6-31G(d) for the family of "closed" (*S*)-**3$_c$** conformers was much higher than expected (91.3%; see Table 1). Apparently, the problem is that the continuum solvation model accounts for bulk solvent effects, but is unsuited to describe the ability of the solvent to directly participate as a hydrogen-bond acceptor/donor, thus leading to a realistic competition between intra- and intermolecular hydrogen bonds.[14] A better description of such a kind of short-range solute–solvent interaction might be achieved by inclusion of explicit solvent molecules, although one may expect that entropy (conformational versus solvent release/engagement) would also play a role in this balance.

Table 1. Single-point M06-2X/6-311+G(d,p) energy calculations on (*S*)-**3** obtained from an implicit solvent model (IEF-PCM) of ACN (geometry optimized at the B3LYP/6-31G(d) level of theory).

Conformer[a]	ΔE[b] [kcal mol^{-1}]	Population [%]	Conformer[a]	ΔE[b] [kcal mol^{-1}]	Population [%]
C1$_c$	7.5	0.0	**C14$_o$**	3.9	0.1
C2$_c$	17.7	0.0	**C15$_c$**	2.1	1.6
C3$_o$	7.6	0.0	**C16$_o$**	8.5	0.0
C4$_c$	6.3	0.0	**C17$_o$**	3.4	0.2
C5$_c$	5.9	0.0	**C18$_c$**	0.9	12.8
C6$_o$	2.3	1.2	**C19$_o$**	1.8	2.8
C7$_o$	2.4	0.9	**C20$_o$**	5.7	0.0
C8$_c$	4.3	0.0	**C21$_c$**	1.1	8.4
C9$_o$	3.5	0.1	**C22$_c$**	0.0	55.7
C10$_o$	5.0	0.0	**C23$_o$**	7.7	0.0
C11$_o$	1.9	2.2	**C24$_c$**	2.8	0.5
C12$_o$	2.2	1.3	**C25$_c$**	0.9	11.9
C13$_c$	3.0	0.3			

[a] o = "open" conformation with no intramolecular hydrogen bonding, c = "closed" conformation with intramolecular hydrogen bonding. [b] Internal energy relative to the lowest-energy conformer.

Therefore, further molecular modeling was performed by including one ACN molecule in the input structures. Among the 13 non-hydrogen-bonded (*S*)-**3$_o$** "open" conformers and the 12 hydrogen-bonded (*S*)-**3$_c$** "closed" conformers obtained from the IEF-PCM calculations (Table 1), the two most stable conformers that belong to each family, namely **C19$_o$** and **C22$_c$** in Table 1, were selected as starting structures for subsequent explicit solvent MC searches. By starting from the non-hydrogen-bonded geometry **C19$_o$**, a structure for the adduct (*S*)-**3$_o$·ACN** was obtained by placing one ACN molecule in the vicinity of the 4a-OH group with a 4a-OH···NCCH$_3$ distance of 2.1 Å (Figure 2). From the hydrogen-bonded geometry **C22$_c$**, two starting structures were generated by positioning ACN at two different orientations designated as (*S*)-**3$_c$·ACN/A** and (*S*)-**3$_c$·ACN/B** (Figure 2). After an iterative MC search, a total of 147 conformations resulted within an energy window of 20 kJ mol^{-1}. More specifically, the initially "open" (*S*)-**3$_o$·ACN** resulted in 37 structures, most of which showed a hydrogen-bonding interaction between the 4a-OH group and ACN. A few conformers lacked any inter- and intramolecular hydrogen bonds, whereas only one conformer showed an intramolecular OH···3′-Ac hydrogen bond.

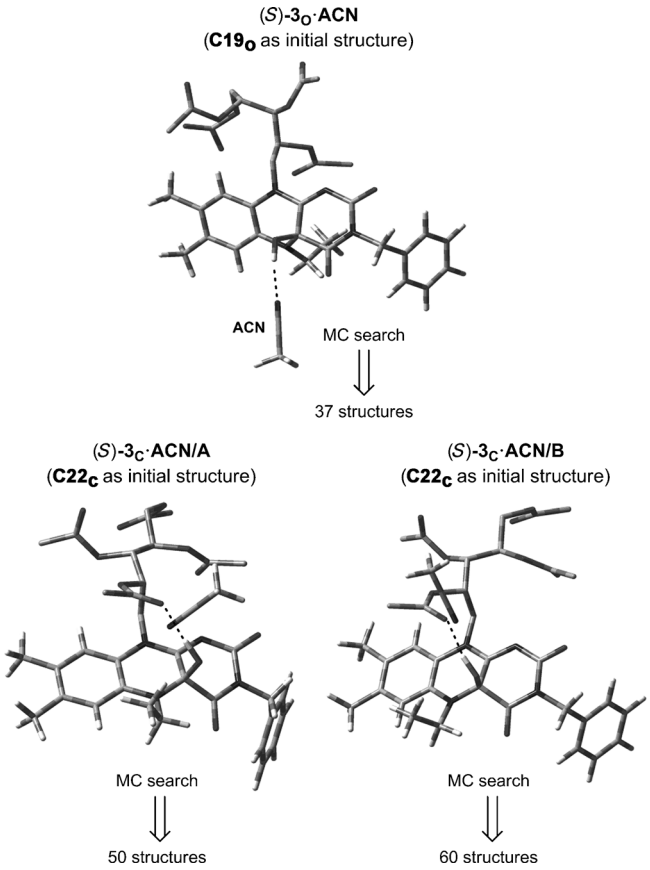

Figure 2. The three starting conformations of (*S*)-**3·ACN** that underwent a MC search with an explicit solvent model for ACN. For clarity of representation, hydrogen atoms have been omitted from the tetraacetyl-D-ribityl backbone. A color version of this figure is given in the Supporting Information.

Among the 50 output structures obtained from the starting "closed" geometry (*S*)-**3$_c$·ACN/A**, most displayed an intermolecular 4a-OH···ACN hydrogen bond, whereas some exhibited an intramolecular 4a-OH···2′-Ac hydrogen bond. On the other

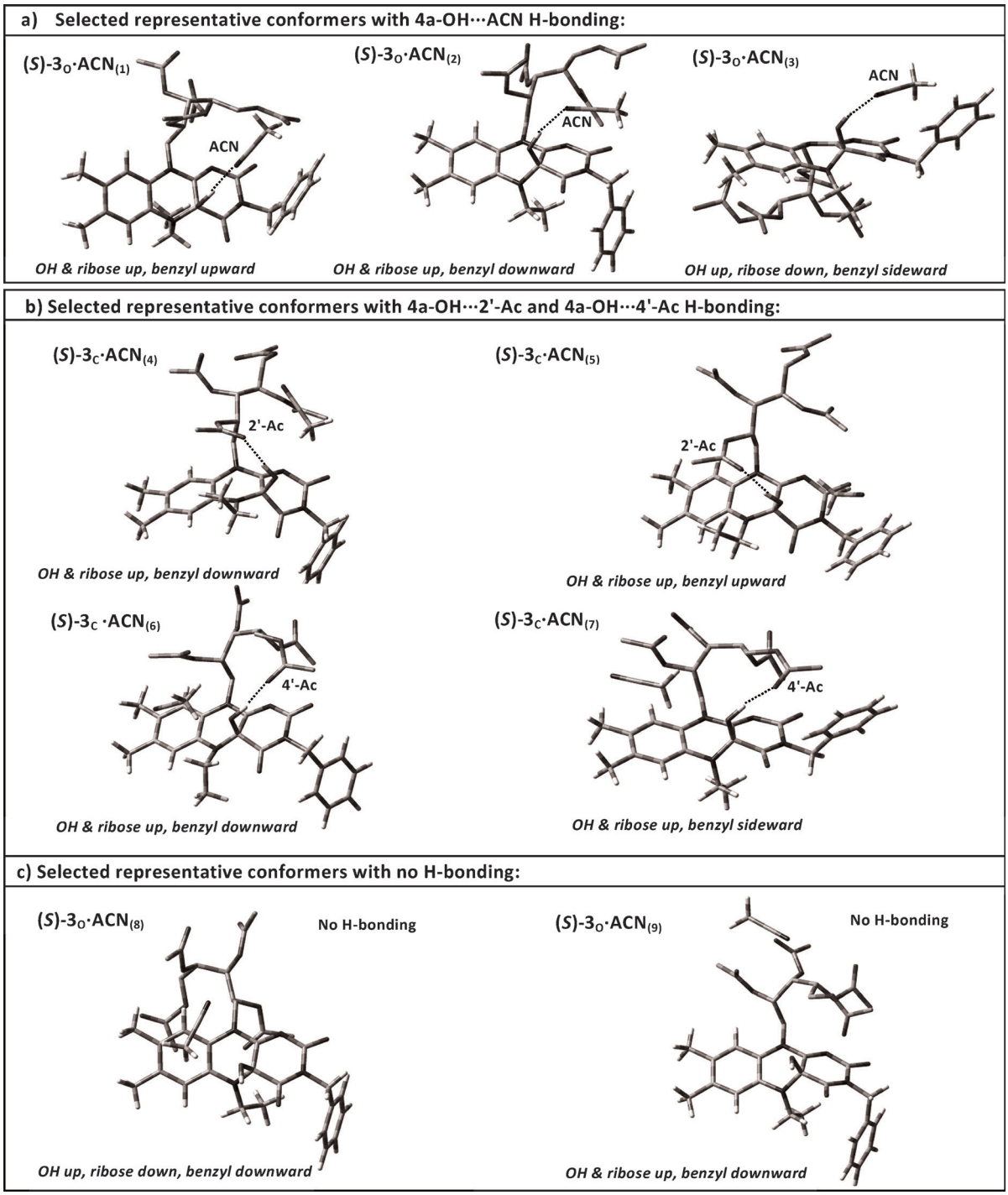

Figure 3. Nine representative conformers with an explicit ACN, obtained from the MC pool of 147, selected based on hydrogen-bonding structural criteria to undergo an initial geometry optimization at the DFT/M06-2X/6-311+G(d,p) level of theory. In addition, the mutual disposition of the OH, ribityl, and benzyl moieties was taken into account. For clarity of representation, the hydrogen atoms have been omitted from the tetraacetyl-D-ribityl backbone. A color version of this figure is given in the Supporting Information.

hand, among the 60 output structures from the starting "closed" geometry (*S*)-**3$_C$·ACN/B**, most retained their intramolecular 4a-OH···4′-Ac hydrogen bonds.

Because it would be impractical to submit the whole ensemble of 147 conformers generated for the (*S*)-**3·ACN** adduct to DFT optimizations, we analyzed these MC conformations in order of increasing energy and selected a few structures that represented the various possible hydrogen-bonding interactions of the 4a-OH group with ACN or an acetyl group (2′-Ac or 4′-Ac), as well as the ones without any hydrogen bonding at all. Additional attention was paid to the relative disposition of the 4a-OH and tetraacetyl-D-ribityl groups and to the orientation of the benzyl group. As a result, we obtained nine representative conformers for the (*S*)-**3·ACN** adducts displayed in Figure 3, which were geometry optimized at the M06-2X/6-311+G(d,p) level to result in the energies listed in Table 2. In-

Table 2. Comparison of the electronic energy for the nine representative conformers shown in Figure 3 (geometry optimized at the M06-2X/6-311+G(d,p) level of theory with explicit solvent model for ACN).

Conformer[a]	$\mathbf{3_o{\cdot}ACN_{(1)}}$	$\mathbf{3_o{\cdot}ACN_{(2)}}$	$\mathbf{3_o{\cdot}ACN_{(3)}}$	$\mathbf{3_c{\cdot}ACN_{(4)}}$	$\mathbf{3_c{\cdot}ACN_{(5)}}$
ΔE[b] [kcal mol^{-1}]	0.00	5.28	1.62	2.33	4.50
Conformer[a]	$\mathbf{3_c{\cdot}ACN_{(6)}}$	$\mathbf{3_c{\cdot}ACN_{(7)}}$	$\mathbf{3_o{\cdot}ACN_{(8)}}$	$\mathbf{3_o{\cdot}ACN_{(9)}}$	
ΔE[b] [kcal mol^{-1}]	6.90	4.53	1.83	7.77	

[a] o = "open" conformation with no intramolecular hydrogen bonding, c = "closed" conformation with intramolecular hydrogen bonding. [b] Internal energy relative to the first listed conformer.

terestingly enough, the most stable structure was an "open" conformer, namely (*S*)-$\mathbf{3_o{\cdot}ACN_{(1)}}$, which lacked any intramolecular hydrogen bonding with the acetyl groups and exhibited instead an intermolecular 4a-OH···ACN hydrogen bond with an H···N distance of 1.87 Å. In this structure, the tetraacetyl-D-ribityl chain and the benzyl group were both oriented on the same side as the 4a-OH group. The second most stable structure was (*S*)-$\mathbf{3_o{\cdot}ACN_{(3)}}$, which also displayed intermolecular 4a-OH···ACN hydrogen bonding, yet with an opposite orientation of the 4a-OH and tetraacetyl-D-ribityl groups. Notably, in both these structures the benzyl moiety was in close vicinity to the methyl group of the ACN molecule, perhaps due to a stabilizing non-bonding interaction between the benzyl and methyl groups. The third structure in order of stability was (*S*)-$\mathbf{3_o{\cdot}ACN_{(8)}}$, without any hydrogen bonding. Among the "closed" conformers, the most stable structure was (*S*)-$\mathbf{3_c{\cdot}ACN_{(4)}}$, with an intramolecular 4a-OH···2′-Ac hydrogen bond, which was higher in energy by 2.33 kcal mol^{-1} than (*S*)-$\mathbf{3_o{\cdot}ACN_{(1)}}$. Although the set of nine selected structures does not necessarily cover the whole conformational ensemble, it clearly indicated a strong preference for structures devoid of intramolecular hydrogen bonds, which was eventually in accord with the experimental results.

TDDFT CD calculations on representative structures of (*S*)-3

The selection of the best functional/basis-set combination for the TDDFT calculations was based on a preliminary screening run on an essential molecular model that represented the 4a-hydroxyflavin chromophore (see the Computational Section). On this model, optimized at the B3LYP/6-31G(d) level, the hybrid functionals B3LYP CAM-B3LYP and M06-2X and the basis sets TZVP, ma-TZVP, and aug-TZVP were tested (see the Computational Section for details). All the combinations gave consistent results. The best functional in terms of agreement with the experimental absorption and CD spectra was CAM-B3LYP; the basis set with the best cost/efficiency compromise was ma-TZVP. The combination CAM-B3LYP/TZVP was selected for the calculations on the relatively large structures of (*S*)-**3·ACN** adducts, whereas the larger basis set ma-TZVP was employed for the simplified model (*S*)-**4** discussed below.

TDDFT calculations were run on the five representative stable structures of (*S*)-**3·ACN** discussed above, namely (*S*)-$\mathbf{3_o{\cdot}ACN_{(1)}}$, (*S*)-$\mathbf{3_o{\cdot}ACN_{(3)}}$, (*S*)-$\mathbf{3_c{\cdot}ACN_{(4)}}$, (*S*)-$\mathbf{3_c{\cdot}ACN_{(5)}}$, and (*S*)-$\mathbf{3_o{\cdot}ACN_{(8)}}$, which cover all the relevant possible hydrogen bonding situations and orientations of the various groups. By considering the chemical structure of (*S*)-**3** and its experimental CD data, it was expected that the conformation of the 4a-hydroxyflavin moiety would be of key importance in determining the calculated CD spectra, which would in turn largely depend on the presence or absence of an intramolecular hydrogen bond between the 4a-OH moiety and one of the acetyl groups. In fact, the three structures (*S*)-$\mathbf{3_o{\cdot}ACN_{(1)}}$, (*S*)-$\mathbf{3_o{\cdot}ACN_{(3)}}$, and (*S*)-$\mathbf{3_o{\cdot}ACN_{(8)}}$ with no intramolecular hydrogen bonds show an essentially identical puckering of the 4a-hydroxyflavin skeleton, whose three rings lie almost coplanar to each other (see Figure 3). Conversely, the two conformers (*S*)-$\mathbf{3_c{\cdot}ACN_{(4)}}$ and (*S*)-$\mathbf{3_c{\cdot}ACN_{(5)}}$, both with 4a-OH···2′-Ac intramolecular hydrogen bond, feature a more distorted 4a-hydroxyflavin moiety.

The CD spectra calculated at the CAM-B3LYP/TZVP level for the five structures are shown in Figure 4. The three structures (*S*)-$\mathbf{3_o{\cdot}ACN_{(1)}}$, (*S*)-$\mathbf{3_o{\cdot}ACN_{(3)}}$, and (*S*)-$\mathbf{3_o{\cdot}ACN_{(8)}}$ gave similar calcu-

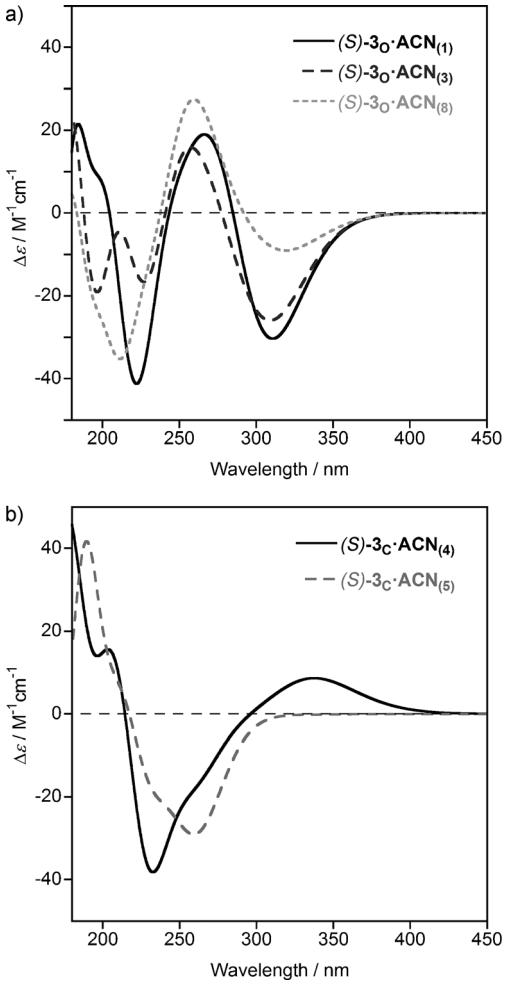

Figure 4. The TDDFT-calculated CD spectra at the CAM-B3LYP/TZVP level for the five representative structures of the (*S*)-**3·ACN** adducts (the geometry was optimized at the M06-2X/6-311+G(d,p) level; see the structures in Figure 3). The rotational strengths computed in the dipole-length gauge were each associated with a Gaussian band-shape with an exponential half-width of 0.4 eV.

lated CD spectra (Figure 4a). The CD profile calculated for the lowest-energy structure (*S*)-**3$_O$·ACN$_{(1)}$** is in especially good agreement with the experimental CD spectrum for the (−)-**3** isomer (Figure 1b) in terms of sign, relative intensities, and positions of the three major bands, despite a systematic wavelength blue-shift of about $\Delta\lambda = 40$ nm; a direct comparison, including absorption spectra, is shown in Figure S4 (see the Supporting Information). On the contrary, the CD spectra calculated for the two structures (*S*)-**3$_C$·ACN$_{(4)}$** and (*S*)-**3$_C$·ACN$_{(5)}$** deviate substantially from the experimental CD profiles (Figure 4b). These results clearly indicated that the conformation assumed by the 4a-hydroxyflavin moiety is a major determinant of the observed and calculated CD spectra. Furthermore, we also considered two simplified structures obtained from the lowest-energy geometry (*S*)-**3$_O$·ACN$_{(1)}$** by subsequent removal of the tetraacetyl-D-ribityl moiety and the ACN molecule. In both cases, the calculated CD spectra were almost superimposable to that of the original (*S*)-**3$_O$·ACN$_{(1)}$** (see Figure S5 in the Supporting Information). This observation demonstrated that both the tetraacetyl-D-ribityl moiety and the ACN molecule have no direct impact on the excited-state calculations. Finally, we noticed that the CD spectra calculated for (*S*)-**3$_O$·ACN$_{(1)}$** and the other representative structures (*S*)-**3$_O$·ACN$_{(3)}$** and (*S*)-**3$_O$·ACN$_{(8)}$** reproduced well the sequence of signs of CD bands observed for the (−)-**3** isomer (compare Figures 1 and 4 or see Figure S4 in the Supporting Information). Therefore, we conclude that the absolute configurations at the 4a position of the diastereomeric 4a-hydroxyflavins (+)- and (−)-**3** should be assigned as the *R* and *S* isomers, respectively.

TDDFT CD calculations on model (*S*)-4

The whole set of the experimental data for (+)-**3** and (−)-**3** and the theoretical data collected for (*S*)-**3** presented above clearly demonstrated a hypothesis, which we anticipated on the basis of stereochemical and spectroscopic reasoning; that is, the CD spectra of these compounds are not affected by the tetraacetyl-D-ribityl moiety attached at the N10 position. First of all, because the tetraacetyl-D-ribityl chain does not contain any strong chromophoric group, it cannot perturb the transitions of the 4a-hydroxyflavin chromophore. Second, the tetraacetyl-D-ribityl chain is unlikely to impact the conformation assumed by the 4a-hydroxyflavin ring because any specific interaction (for example, an intramolecular hydrogen bond) would lead to a thermodynamically unstable medium-size cycle (see the discussion below). As a consequence, the hypothetical compound (*S*)-**4** (Figure 5), in which the tetraacetyl-D-ribityl group has been cut away and replaced by a "capping" methyl group, should represent a valid candidate model to interpret the stereochemical information contained in the CD spectra of (+)-**3** and (−)-**3**. Because most of the molecular flexibility of (+)-**3** and (−)-**3** is confined to the tetraacetyl-D-ribityl side chain, the model dramatically simplified the molecular-modeling and CD-calculation steps.[15] In fact, as a result of MMFF conformational searches followed by B3LYP/6-31G(d) geometry optimizations in vacuo (see the Computational Section for details), only two populated conformations at room temperature

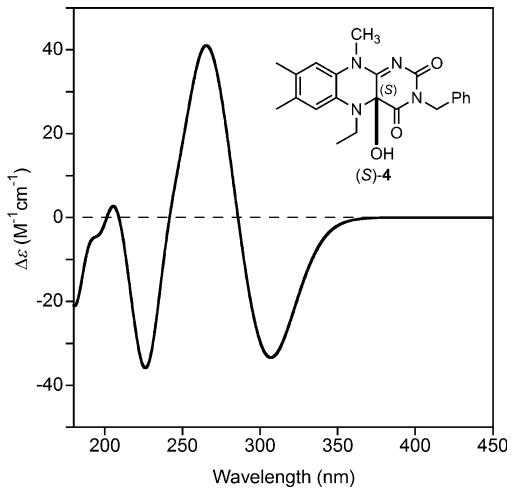

Figure 5. The TDDFT-calculated CD spectrum at the CAM-B3LYP/ma-TZVP level on the model compound (*S*)-**4** (see inset) obtained as a Boltzmann-weighted average at 300 K for the two minima optimized at the B3LYP/6-31G(d) level. The rotational strengths computed in the dipole-length gauge were each associated with a Gaussian band-shape with an exponential half-width of 0.3 eV.

resulted for (*S*)-**4** (see Figure S6 in the Supporting Information). These structures differed only in the orientation of the benzyl group, whereas the conformation assumed by the 4a-hydroxyflavin ring was almost planar, similar to the lowest-energy structure (*S*)-**3$_O$·ACN$_{(1)}$** found for the (*S*)-**3·ACN** adduct. The CD spectra calculated at the CAM-B3LYP/ma-TZVP level for the two conformations were very similar to each other. The Boltzmann-weighted average of these conformers at 300 K (Figure 5) revealed a very close similarity to the CD spectrum calculated for (*S*)-**3$_O$·ACN$_{(1)}$** (Figure 4) and to that observed for (−)-**3** (Figure 1; a direct comparison is shown in Figure S7 in see the Supporting Information). In practice, consideration of model (*S*)-**4** would lead to the same configurational assignment reached above, but with a much reduced computational effort.

On this model, it was also easier to assign the main observed CD bands by means of orbital and population analysis. It turned out that the two major bands in the region of $\lambda =$ 260–400 nm are allied to two π–π^* transitions both localized on the 4a-hydroxyflavin chromophore and endowed with some charge-transfer character from the benzene ring to the uracil-like ring.

Discussion

Although the main target of our investigation was the absolute configurational assignment of 4a-hydroxyflavin diastereomers **3** mentioned above, there are some important additional aspects that we would like to discuss shortly in the present section.

The foremost problem concerns the evaluation of the most representative conformers that one should consider for predicting CD or other chiroptical properties by means of quantum-mechanics methods such as TDDFT. As mentioned earlier,

preliminary computational data obtained by using the intact molecule (*S*)-**3** in the gas phase followed by an implicit PCM solvent model resulted in the presence of an intramolecular hydrogen bond between the 4a-OH moiety and one of the acetyl groups. This outcome was at odds with simple chemical reasoning and the experimental VT-NMR and CD spectroscopic data in ACN. More specifically, an intramolecular hydrogen bond between the 4a-OH and the acetyl groups at the 2′ or 4′ position of the tetraacetyl-D-ribityl side chain leads to the formation of 10- or 12-membered cycles, respectively, which are energetically disfavored medium-size rings. The conformational entropy associated with these ring-closure processes may not be entirely captured by frequency calculations run on single structures because a correct evaluation would require evaluation of a large statistical ensemble. Moreover, the formation of the hydrogen-bonded cycles also forces the 4a-hydroxyflavin moiety to adopt a distorted "unnatural" conformation (see, for example, structures for (*S*)-$\mathbf{3_C{\cdot}ACN_{(4)}}$ and (*S*)-$\mathbf{3_C{\cdot}ACN_{(5)}}$ in Figure 3), which is likely to occur only in the artificial environment of computational simulations. This apparent computational artifact was not unveiled even with the use of a new-generation functional M06-2X, which is thought to be more accurate than the classical B3LYP in describing hydrogen-bonding interactions.[16] As implied earlier, although an implicit PCM solvent model is adequate for describing bulk solvent effects,[17] it may be ineffective when specific short-range solute–solvent interactions have a relevant impact.[18] In the present investigation, the apparent stabilization of (*S*)-$\mathbf{3_C}$ conformers held together by intramolecular hydrogen bonds warned against the inadequacy of the continuum solvation model and called for further computational analysis. In fact, only the use of an explicit solvent model resolved the discrepancy associated with intramolecular hydrogen bonding by favoring intermolecular hydrogen bonding between the 4a-OH group and ACN.

A discussion worth mentioning concerns the compromise between completeness and simplicity, which is well represented herein by the problem of solvation. In this respect, we have considered that a truly complete computational model would consist of the solute surrounded by a certain number of solvent molecules, yet this protocol is still out of the reach of most ab initio calculations as far as excited states are concerned. Luckily, in the present case, a single explicit solvent molecule reconciled the difference between the molecule in the gas phase (or in polarizable continuum) and in the real solvent. In many cases, as in the present one, electronic CD spectroscopic analysis may offer itself a proof of internal consistency because the CD spectrum consists of several bands; therefore, the experimental and calculated absorption and CD spectra should be compared in terms of global appearance, thus not limited to the sign of the first or few CD bands. In fact, the CD spectra calculated for the two "suspicious" structures (*S*)-$\mathbf{3_C{\cdot}ACN_{(4)}}$ and (*S*)-$\mathbf{3_C{\cdot}ACN_{(5)}}$ (Figure 4B) had overall profiles very different from the experimental one (i.e., the CD spectrum of (−)-**3** in Figure 1).

The simplification from compound **3** to **4** corresponds to a so-called "truncation approach" for the analysis of CD spectra. In this approach, the molecule under investigation is "pruned" at each "branch", which is envisaged not to affect in any sizable way the observed chiroptical response, and the CD prediction is then run on the simplified truncated model. The method is particularly well suited for electronic CD spectroscopy, which responds primarily to chromophores and their immediate environment and is less sensitive to spectroscopically silent molecular portions.[19] The truncated analogue **4** incorporates the prior knowledge that intramolecular hydrogen bonding does not exist and gives rise to a straightforward conformation analysis, which is focused on the spectroscopically relevant molecular portion. The use of a truncated model may greatly simplify the analysis, but it represents a double-edged sword because it is based on the assumption, which needs to be verified, that the "pruned branches" do not contribute to the CD spectrum in any way, either directly, by perturbing chromophore transitions, or indirectly, by impacting on its structure. An example that makes evident the caution to be paid in the use of truncated models is the study on gymnocin B, in which the attempt to truncate a molecular "tail" led to erroneous conformational results.[20] On the other hand, when it is successful,[21] this double-edged sword allows one to doubly reduce computational effort, that is, for the conformation analysis and for the excited-state calculations necessary to predict electronic CD. In the current case, the use of truncated model (*S*)-**4** would apparently provide the right answer for the right reason, that is, the neglect of any effect exerted by the tetraacetyl-D-ribityl side chain on the 4a-hydroxyflavin core.

Conclusion

Determination of the absolute configuration of an organic compound by means of quantum-mechanical calculations of chiroptical spectra, such as electronic CD spectroscopy, necessarily relies on the detailed knowledge of a molecular geometry. Because CD spectroscopic measurements are most often run in solution, the resulting conformational ensemble observed in the presence of a particular solvent must be known with accuracy. Herein, we have reported a thorough CD study on the 4a-hydroxyflavin derivative **3** of flavin analogue **1**, which was previously obtained as a diastereomeric mixture and separated into diastereomers (+)-**3** and (−)-**3** by HPLC. The molecular structure of **3** includes an intrinsically chiral chromophore, the 4a-hydroxyflavin, attached at the N10 position to a tetraacetyl-D-ribityl substituent, which itself is chiral, non-chromophoric, and very flexible. The collection of experimental and computational data demonstrated that the tetraacetyl-D-ribityl chain does not affect the conformation and electronic transitions of the 4a-hydroxyflavin chromophore to any extent. We have also demonstrated that two alternative approaches could be used to reproduce the CD spectrum of (−)-**3** by TDDFT calculations and to assign its configuration. In the first approach, a thorough conformation analysis was run on the whole molecular structure. Importantly, the results of the conformation analysis in the gas phase or implicit solvent environment were at odds with the experimental observations. Further analysis by including one explicit solvent molecule

(i.e., ACN) in the calculations proved to be necessary to obtain good agreement between the theoretical and experimental CD spectroscopic data. In the second approach, the tetraacetyl-D-ribityl chain was truncated and the simplified model **4** was considered. In both cases, calculated CD spectra by using TDDFT led to a reliable assignment of the absolute configurations of (+)-**3** and (−)-**3** as (*R*)-**3** and (*S*)-**3** isomers, respectively.

The present configurational assignment of a 4a-hydroxyflavin may be valid for the analogue 4a-hydroperoxyflavin, the key intermediate responsible for diverse transformation reactions catalyzed by a large family of flavoenzymes and synthetic flavin derivatives. The results will not only provide new insight into the molecular basis mechanism of flavin-catalyzed reactions but also open possibilities for the design and synthesis of novel flavin-based asymmetric organocatalysts.

Experimental Section

Separation of (+)-3 and (−)-3

The 4a-hydroxyflavin **3** was separated into diastereomers (+)-**3** and (−)-**3** on a chiral HPLC column (Chiralpak IB, 2 (i.d.) × 25 cm, *n*-hexane/$CHCl_3$ = 1:1 (v/v), 5.5 mL min^{-1}) or an HPLC column (Cosmosil 5C18-MS-II, 2.8 (i.d.) × 25 cm, ACN/H_2O = 11:9 (v/v), 12 mL min^{-1}). The prefixes + and − denote the signs of the optical rotation at the sodium D-line. The ^{1}H NMR spectra of **3** showed two sets of peaks attributed to the diastereomeric pair (+)-**3** and (−)-**3**, and the diastereomeric excess values of (+)-**3** and (−)-**3** were estimated to be 94% *de* (see Figures S1 B–D in the Supporting Information). The molar ellipticity $\Delta\varepsilon$ values at the first, second, and third Cotton effects were $\Delta\varepsilon = 9.55$, −13.8, and 14.25 ($\lambda = 348$, 284, and 240 nm), respectively, for (+)-**3** and $\Delta\varepsilon = -11.07$, 12.94, and −17.00 ($\lambda = 346$, 285, and 241 nm), respectively, for (−)-**3** (Figure 1).

Computational Section

Molecular modeling: The initial survey of the potential-energy surface (PES) was performed by using a molecular-mechanics Monte Carlo (MC) algorithm in the gas phase and employing three conformational search methods within the MacroModel applet of Schrodinger software:[22] 1) Monte Carlo multiple minimum (MCMM), 2) systematic pseudo-Monte Carlo (SPMC), and 3) mixed torsional/Larges-scale low-mode sampling. Each search was set to 10000 steps for (*S*)-**3** treated in vacuo (gas phase). The minimization method used was the polar-Ribiere conjugate gradient (PRCG), with 1000 iteration steps to reach the minimum. All three of the MC searches were performed at both OPLS-2005 and MMFFs force fields to ensure a thorough PES search, regardless of the parameterization. The search was considered to be converged, and hence complete, once iterative MC submission provided no further lower-energy conformations. Independently, each of the six MC searches resulted in approximately 3000 conformers. The redundant conformers from the six composite searches were eliminated on this basis: 1) a distance cutoff of 7 Å for all atoms and 2) an energy window of 20 kJ mol^{-1}. As a result of the redundant-conformer elimination, 25 conformers were identified. DFT calculations were run with the Gaussian09 program[23] with default grids and convergence criteria. DFT geometry optimization and frequency calculations were performed under the following two levels of theory:[24] B3LYP/6–31G(d), M06–2X/6–311 + G(d,p) geometry optimization in the gas phase and M06–2X/6–311 + G(d,p) geometry optimization with explicit ACN. The M06–2X/6–311 + G(d,p) single-point energy calculations were carried out under an implicit (IEF-PCM) ACN solvent environment, with Gaussian09 default parameters. Due to the size of the system and the level of the theory, we used a more cost-effective approach by submitting all 25 conformers from the M06–2X/6–311 + G(d,p) geometry optimization in the gas phase to a single-point energy calculation, rather than the full geometry optimization. The calculation was performed under an implicit account for the solvent presence by using the IEF-PCM method.

Excited-state calculations: The TDDFT calculations were run with Gaussian09 with default grids and without any implicit solvent model. Several hybrid DFT functionals (B3LYP, CAM-B3LYP, M06–2X) and basis sets (TZVP, ma-TZVP, aug-TZVP)[24] were initially tested on an essential molecular model that represented the 4a-hydroxyflavin chromophore, which was obtained by replacing both tetraacetyl-D-ribityl and benzyl groups in (*S*)-**3** with two methyl groups. The two augmented basis sets were constructed by adding to the standard Ahlrichs TZVP basis set, a set of (1p1d) diffuse functions (ma-TZVP)[25] or a set of (1s1p1d/1s1p) diffuse functions taken from the most diffuse functions of aug-cc-pVDZ (aug-TZVP),[26] respectively. The final calculations were run with CAM-B3LYP/TZVP on (*S*)-**3·ACN** adducts, including 48 excited states, and with CAM-B3LYP/ma-TZVP on the truncated model (*S*)-**4**, including 36 excited states. Electronic CD spectra were generated with the program Specdis[27] by applying a Gaussian band shape with an exponential half-width of 0.3–0.4 eV by using dipole-length rotational strengths; the difference in the dipole–velocity values was checked to be minimal for all the relevant transitions.

Acknowledgements

The authors thank Prof. Koji Nakanishi for his helpful discussion and suggestions. This research was supported in part by a Grant-in-Aid for Young Scientists (B) (H.I.) from the Japan Society for the Promotion of Science (JSPS) and in part by the Italian Ministero dell'Istruzione, dell'Università e della Ricerca (MIUR), "Progetto PRIN 2009 prot. 2009PRAM8L". S.I. is grateful for a JSPS Research Fellowship for Young Scientists (no. 4919), the Institutional Program for Young Researcher Overseas Visits from JSPS, and to Prof. K. Nakanishi for his hospitality during his stay at Columbia University during 2012–2013. N.B. appreciates the instrumental and technical support of JASCO Corp., (Japan) and JASCO, Inc. (USA).

Keywords: circular dichroism · conformation analysis · hydrogen bonds · solvent effects · structure elucidation

[1] a) T. C. Bruice, *Acc. Chem. Res.* **1980**, *13*, 256–262; b) V. Massey, *Biochem. Soc. Trans.* **2000**, *28*, 283–296; c) F. Müller, *Chemistry and Biochemistry of Flavoenzymes*, CRC Press, Boston, **1991**; d) C. Walsh, *Acc. Chem. Res.* **1980**, *13*, 148–155.

[2] a) N. B. Beaty, D. P. Ballou, *J. Biol. Chem.* **1981**, *256*, 4619–4625; b) J. R. Cashman, *Chem. Res. Toxicol.* **1995**, *8*, 165–181; c) L. L. Poulsen, D. M. Ziegler, *J. Biol. Chem.* **1979**, *254*, 6449–6455; d) D. M. Ziegler, *Drug Metab. Rev.* **2002**, *34*, 503–511; e) K. C. Jones, D. P. Ballou, *J. Biol. Chem.* **1986**, *261*, 2553–2559.

[3] The half-life of FlOOH has been estimated to be as low as 2.5 ms: a) R. F. Anderson, in *Flavins and Flavoproteins* (Eds.: R. C. Bray, P. C. Engel and S. E. Mayhew), DeGruyter, Berlin, **1984**, ch. 57–60. Recently, 4a–oxygen adducts (either FlOOH or FlOH) were reported to be present as an intermediate in choline oxidase and pyranose dehydrogenase by crystallographic analysis: b) A. M. Orville, G. T. Lountos, S. Finnegan, G. Gadda, R. Prabhakar, *Biochemistry* **2009**, *48*, 720–728; c) T. C. Tan, O.

Spadiut, T. Wongnate, J. Sucharitakul, I. Krondorfer, C. Sygmund, D. Haltrich, P. Chaiyen, C. K. Peterbauer, C. Divne, *PLoS One* **2013**, *8*, e53567.

[4] a) G. de Gonzalo, M. W. Fraaije, *ChemCatChem* **2013**, *5*, 403 – 415; b) F. G. Gelalcha, *Chem. Rev.* **2007**, *107*, 3338 – 3361; c) Y. Imada, T. Naota, *Chem. Rec.* **2007**, *7*, 354 – 361.

[5] C. Kemal, T. C. Bruice, *Proc. Natl. Acad. Sci. USA* **1976**, *73*, 995 – 999.

[6] S.-I. Murahashi, T. Oda, Y. Masui, *J. Am. Chem. Soc.* **1989**, *111*, 5002 – 5003.

[7] For examples of 1- or 5-alkylated flavin catalysts, see: a) K. Bergstad, J.-E. Bäckvall, *J. Org. Chem.* **1998**, *63*, 6650 – 6655; b) S. Chen, M. S. Hossain, F. W. Foss, *Org. Lett.* **2012**, *14*, 2806 – 2809; c) Y. Imada, H. Iida, T. Kitagawa, T. Naota, *Chem. Eur. J.* **2011**, *17*, 5908 – 5920; d) Y. Imada, H. Iida, S.-I. Murahashi, T. Naota, *Angew. Chem.* **2005**, *117*, 1732 – 1734; *Angew. Chem. Int. Ed.* **2005**, *44*, 1704 – 1706; e) Y. Imada, H. Iida, T. Naota, *J. Am. Chem. Soc.* **2005**, *127*, 14544 – 14545; f) Y. Imada, H. Iida, S. Ono, S.-I. Murahashi, *J. Am. Chem. Soc.* **2003**, *125*, 2868 – 2869; g) A. A. Linden, L. Krueger, J.-E. Bäckvall, *J. Org. Chem.* **2003**, *68*, 5890 – 5896; h) B. J. Marsh, E. L. Heath, D. R. Carbery, *Chem. Commun.* **2011**, *47*, 280 – 282; i) C. Mazzini, J. Lebreton, R. Furstoss, *J. Org. Chem.* **1996**, *61*, 8 – 9; j) A. B. E. Minidis, J.-E. Bäckvall, *Chem. Eur. J.* **2001**, *7*, 297 – 302. For examples of chiral flavin-catalyzed asymmetric oxidations, see: k) R. Jurok, R. Cibulka, H. Dvorakova, F. Hampl, J. Hodacova, *Eur. J. Org. Chem.* **2010**, 5217 – 5224; l) V. Mojr, M. Budesinsky, R. Cibulka, T. Kraus, *Org. Biomol. Chem.* **2011**, *9*, 7318 – 7326; m) S.-I. Murahashi, *Angew. Chem.* **1995**, *107*, 2670 – 2693; *Angew. Chem. Int. Ed. Eng.* **1995**, *34*, 2443 – 2465; n) S.-I. Murahashi, S. Ono, Y. Imada, *Angew. Chem.* **2002**, *114*, 2472 – 2474; *Angew. Chem. Int. Ed.* **2002**, *41*, 2366 – 2368; o) S. Shinkai, T. Yamaguchi, A. Kawase, O. Manabe, R. M. Kellogg, *J. Am. Chem. Soc.* **1989**, *111*, 4935 – 4940; p) S. Shinkai, T. Yamaguchi, O. Manabe, F. Toda, *J. Chem. Soc. Chem. Commun.* **1988**, 1399 – 1401.

[8] H. Iida, S. Iwahana, T. Mizoguchi, E. Yashima, *J. Am. Chem. Soc.* **2012**, *134*, 15103 – 15113.

[9] A close inspection of the reported crystallographic data of 4a–oxygen adducts (either FlOOH or FlOH) in choline oxidase (see ref. [3b]) and pyranose dehydrogenase (see ref. [3c]) indicates that the 4a–oxygen adducts may have the *R* configurations, although the uncertainty of the crystal structures could not discriminate between the FlOOH and FlOH structures.

[10] a) B. R. Leeflang, J. F. G. Vliegenthart, L. M. J. Kroonbatenburg, B. P. Vaneijck, J. Kroon, *Carbohydr. Res.* **1992**, *230*, 41 – 61; b) K. D. Zhang, R. B. Teklebrhan, G. Schreckenbach, S. Wetmore, F. Schweizer, *J. Org. Chem.* **2009**, *74*, 3735 – 3743.

[11] C. A. Hunter, *Angew. Chem.* **2004**, *116*, 5424 – 5439; *Angew. Chem. Int. Ed.* **2004**, *43*, 5310 – 5324.

[12] G. Pescitelli, L. Di Bari, N. Berova, *Chem. Soc. Rev.* **2011**, *40*, 4603 – 4625.

[13] a) M. Ebitani, Y. In, T. Ishida, K.-i. Sakaguchi, J. L. Flippen-Anderson, I. L. Karle, *Acta Crystallogr. Sect. B* **1993**, *49*, 136 – 144; b) P. Ménová, V. Eigner, J. Čejka, H. Dvořáková, M. Šanda, R. Cibulka, *J. Mol. Struct.* **2011**, *1004*, 178 – 187.

[14] B. Mennucci, R. Cammi, *Continuum Solvation Models in Chemical Physics: From Theory to Applications*, Wiley, Chichester, **2007**.

[15] It must be stressed that the following analysis is based on model (*S*)-**4** treated as an independent molecule; thus, the structures of this compound were not derived by the truncation of optimized structures of (*S*)-**3**, but found by independent molecular modeling and DFT calculations.

[16] Y. Zhao, D. Truhlar, *Theor. Chem. Acc.* **2008**, *119*, 525 – 525.

[17] B. Mennucci, C. Cappelli, R. Cammi, J. Tomasi, *Chirality* **2011**, *23*, 717 – 729.

[18] a) V. P. Nicu, E. J. Baerends, P. L. Polavarapu, *J. Phys. Chem. A* **2012**, *116*, 8366 – 8373; b) F. Lipparini, F. Egidi, C. Cappelli, V. Barone, *J. Chem. Theory Comput.* **2013**, *9*, 1880 – 1884.

[19] a) N. Berova, L. Di Bari, G. Pescitelli, *Chem. Soc. Rev.* **2007**, *36*, 914 – 931; b) G. Snatzke, *Angew. Chem.* **1979**, *91*, 380 – 393; *Angew. Chem. Int. Ed. Eng.* **1979**, *18*, 363 – 377.

[20] K. Tanaka, Y. Itagaki, M. Satake, H. Naoki, T. Yasumoto, K. Nakanishi, N. Berova, *J. Am. Chem. Soc.* **2005**, *127*, 9561 – 9570.

[21] a) X.-W. Shi, A.-L. Zhang, G. Pescitelli, J.-M. Gao, *Chirality* **2012**, *24*, 386 – 390; b) J. M. Dragna, G. Pescitelli, L. Tran, V. M. Lynch, E. V. Anslyn, L. Di Bari, *J. Am. Chem. Soc.* **2012**, *134*, 4398 – 4407.

[22] Schrödinger Suite 2012: Macromodel, version 9.9. New York NY, **2012**.

[23] Gaussian 09, Revision C.01. M. J. Frisch, G. W. Trucks, H. B. Schlegel, G. E. Scuseria, M. A. Robb, J. R. Cheeseman, G. Scalmani, V. Barone, B. Mennucci, G. A. Petersson, H. Nakatsuji, M. Caricato, X. Li, H. P. Hratchian, A. F. Izmaylov, J. Bloino, G. Zheng, J. L. Sonnenberg, M. Hada, M. Ehara, K. Toyota, R. Fukuda, J. Hasegawa, M. Ishida, T. Nakajima, Y. Honda, O. Kitao, H. Nakai, T. Vreven, J. A. Montgomery, J. E. Peralta, F. Ogliaro, M. Bearpark, J. J. Heyd, E. Brothers, K. N. Kudin, V. N. Staroverov, R. Kobayashi, J. Normand, K. Raghavachari, A. Rendell, J. C. Burant, S. S. Iyengar, J. Tomasi, M. Cossi, N. Rega, J. M. Millam, M. Klene, J. E. Knox, J. B. Cross, V. Bakken, C. Adamo, J. Jaramillo, R. Gomperts, R. E. Stratmann, O. Yazyev, A. J. Austin, R. Cammi, C. Pomelli, J. W. Ochterski, R. L. Martin, K. Morokuma, V. G. Zakrzewski, G. A. Voth, P. Salvador, J. J. Dannenberg, S. Dapprich, A. D. Daniels, Farkas, J. B. Foresman, J. V. Ortiz, J. Cioslowski, D. J. Fox. Wallingford CT, **2009**.

[24] All references about DFT functionals and basis sets can be found in the online documentation for Gaussian09 at www.gaussian.com/g tech/g ur/g09 help.htm.

[25] J. Zheng, X. Xu, D. Truhlar, *Theor. Chem. Acc.* **2011**, *128*, 295 – 305.

[26] R. A. Kendall, J. T. H. Dunning, R. J. Harrison, *J. Chem. Phys.* **1992**, *96*, 6796 – 6806.

[27] a) Specdis v. 1.60. T. Bruhn, Y. Hemberger, A. Schaumlöffel, G. Bringmann. University of Würzburg (Germany), **2012**; b) T. Bruhn, A. Schaumlöffel, Y. Hemberger, G. Bringmann, *Chirality* **2013**, *25*, 243 – 249.

Received: November 8, 2013
Published online on March 3, 2014

